Lower Atmospheric Signatures During Solar Flares Associated with Seismicity

Jamie Ryan
Mullard Space Science Laboratory
University College London
Surrey, RH13 6NL, UK
jamie.ryan.14@ucl.ac.uk

Contents

1 Data and Methodology

1.1 Observations

The X1 flare of the 29th of March 2014 in active region NOAA 12017, was well observed by RHESSI, IRIS and SDO/HMI, collecting HXR, UV and optical emission respectively. The peak of the impulsive phase of the flare occurs at 17:48 UT, at which point all mentioned instruments provide good coverage.

1.1.1 RHESSI

The RHESSI spacecraft is capable of observing a wide range of high energy emission from solar flares, covering soft x-ray to gamma-rays.

RHESSI captured a wide range of high energy emission throughout the flare, however, for this project, only the 10 to 100 keV HXR range are sampled. During the impulsive phase of a flare, high energy x-ray emission is an indicator that accelerated particles are present. Assuming that the chromosphere is a thick target (Brown, 1971), the deposition of energy by accelerated particles is due to collisions between charged particles and ions producing hard X-ray bremsstrahlung emission. Using equation 1 one can calculate the power, P, injected into the atmosphere by non-thermal electrons.

$$P(E \geq E_c) = \int_{E_C}^{\infty} EF(E)dE \tag{1}$$

The electron distribution $F(E)$ is controlled by the power law $AE^{-\delta}$, where E is the electron energy, A is the total injected electron rate normalisation factor, E_C is the low energy cut off and δ is the electron distribution spectral index. The value of E_C represents the upper boundary between thermal and non-thermal energy contributions to the x-ray spectrum. This means that the total energy associated with non-thermal electron power is a lower limit. Performing the integral in equation 1 gives the total non-thermal electron power in the form of equation 2.

$$P(E \geq E_c) = \frac{AE_C^{(2-\delta)}}{(\delta - 2)} \tag{2}$$

Once P has been determined, a total energy can be calculated by multiplying the power by the time period over which the data covers. In this case that would be the impulsive phase of the flare.

Practically applying a thick target model fit to RHESSI data is acheived by using the `ospex` software within SolarSoft (SSWIDL). The entire data set has to be split into short intervals to improve the accuracy of fitting and the detail of resulting plots. The attenuator state of the instrument has to be taken into account due to differences in sensitivity to incoming photons. Therefore it is important to define intervals for fitting first by the attenuator state as `ospex` will mitigate for the differences in count sensitivity. Then each attenuator time period can be split further in to smaller time increments. Shown in Figure 1 is the resulting fit over the impulsive phase of the flare. At the peak of the impulsive phase between 17:46 and 17:48 the RHESSI fit shows an energy ranging from 1.0×10^{28} to 2.5×10^{29} erg. Assuming the fitting model is correct then the release of this energy is due to non-thermal electrons being accelerated by magnetic reconnection, depositing their energy into the chromosphere.

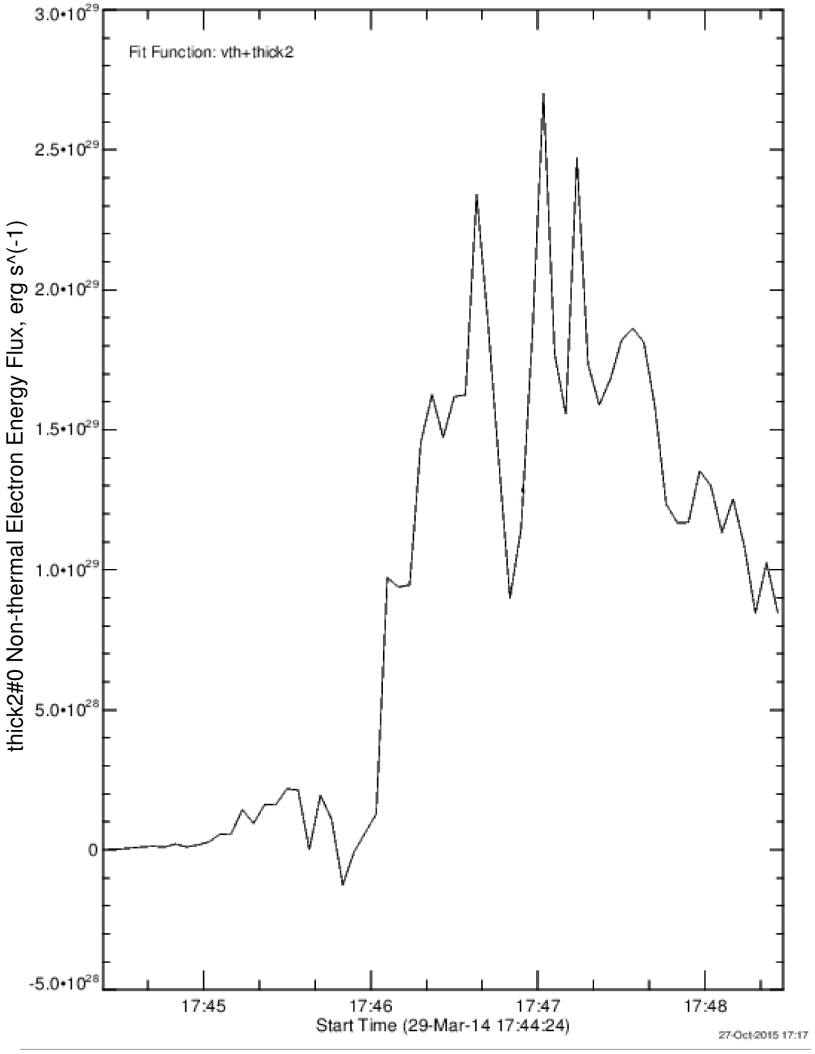

Figure 1: Shows the energy evolution of hard x-ray emission collected by RHESSI 10 to 100 keV bins. Energy units are calculated by fitting a non-thermal electron model to the data.

1.1.2 IRIS

The IRIS spacecraft captured the temporal evolution of the flare between 14:09 and 17:54 UT via it's slit-jaw imager and spectrograph at solar coordinates 491", 282", with a spatial resolution of 0.1667" per pixel. The slit-jaw imager data provides coverage of a field of view spanning 167" by 174", of passbands that including 1403, 2796 and 2832 Å at 26, 19 and 75 second cadence respectively. The spectrograph slit has a field of view spanning 14" by 174" and is aligned directly over chromospheric flare ribbons, and the sunquake point of origin. For the majority of the observation, the spectrograph slit is exposed for $\sim$ 9 seconds at 8 slit locations for a total of 72 seconds cadence per raster. However, during the impulsive phase the IRIS SG shortens it's exposure time to around 2.4 seconds in order to mitigate against saturation of the CCD. Wavelengths observed over three channels include FUV1: 1331.7 - 1358.4 Å, FUV2: 1389.0 - 1407.0 Å and NUV: 2782.7 - 2851.1 Å, associated with the transition region, chromosphere and the upper-photosphere. Spectral lines include C II, Si IV and Mg II h and k. IRIS SJI data is the standard level 2 data product provided for scientific research, which has been calibrated to negate dark currents, flat-field and spacecraft rotational effects. In order to observe flare ribbons in the photospheric data captured by IRIS SJI MG II wing channel, a running difference filter is applyed. This effectively removes unwanted background features, highlighting the UV ribbons. IRIS SG data is manually corrected for changing exposure times and wavelength shifts caused by the orbital motions of the spacecraft. IRIS SG data is sampled over a wavelength range of 2825.7 and 2825.8Å which represents a sample of Balmer pseudo-continuum. The next stage of the processing requires that IRIS SJ and SG data are converted from relative intensity (DN per pixel) to energy (erg) units. This is acheived by using a method provided in the

instrument documentation (De Pontieu et al., 2014) which calculates the conversion factors between DN and erg units in SSWIDL. It is then a case of inserting IRIS DN per pixel intensity values into the equation 3 converting them into energy units. F_{DN} is flux in units of DN per pixel, C_{d2p} is the DN to photon conversion factor, E_λ is the photon energy and E_{erg} is to put the result into erg units.

$$E = \frac{F_{DN} C_{d2p} E_\lambda}{E_{erg}} \tag{3}$$

1.1.3 SDO HMI

The HMI instrument onboard SDO observes the entire solar photosphere, collecting 6173 Å (Fe I) continuum intensity data. HMI has 4k resolution with a pixel size relating to 0.505" spatial resolution, with each image having a cadence of 45 seconds. The data is calibrated to negate cosmic-rays, dark currents, flat-field and spacecraft rotational effects. HMI continuum data is used primarily to observe White light flares, which are difficult to see against the bright photospheric background. To highlight the positions of flare ribbons in the photosphere, data must be filtered. Silimarly to Kerr and Fletcher (2014), photospheric continuum data captured by HMI is put through a two stage filtering porcedure. First the data has an unsharp filter applied, so that the filtered image, $I_{filt} = I -$ smooth(I,10), where I is the original image and the function smooth relates to a 10 pixel boxcar smoothing filter, this is to remove small features such as granulation. The technique is not perfect meaning that some granulation is still visible after the unsharp filter. Second, I_{filt} is subjected to a running difference filter to isolate locations that are white-light enhanced. The running difference filter effectively removes static features leaving behind those pixels that are changing over short time-scales. However, for removing signatures of those processes occurring over shorter time periods such as the remaining granulation and also p-mode oscillations, this filtering technique is ineffective. This is not a problem, as for the purpose of white light flare analysis, the data yield a strong contrast between flare-enhanced and background pixels after being filtered by a $i - 2$ running difference. The next stage is to determine which pixels in the difference image are those that are enhanced during the flare. For the best result, white-light enhanced pixels are identified using a combination of visual inspection and thresholding. Attempts at automating the identification process tend to lead to false positives being triggered by noise or granulation features.
HMI Dopplergrams are used in conjunction with holography techniques to produce a 6mHZ acoustic egression power map (supplied via private communication by Sergei Zharkov) revealing the location of the sunquake. As with the IRIS data, the next stage of processing is to calculate and energy. To perform the energy conversion for SDO HMI data a combination of sources (Boerner et al., 2012; Couvidat et al., 2012) have been used to find the instrument's properties which are used to fulfil a conversion factor in the form of equation 4. Where g is the instrument gain, QE is the quantum efficiency of the charged couple device and A_{ap} is the instrument aperture area, all other terms hold the same meaning as in equation 3.

$$E = \frac{F_{DN} E_\lambda}{g Q E A_{ap} E_{erg}} \tag{4}$$

1.2 Data Sampling

For the IRIS SJI, IRIS SG and SDO HMI data sets, multiple sample points have been chosen based on the moment in time when the IRIS SG slit is directly over the southern flare ribbon and sunquake impact location. These coordinates are sampled across all data sets except RHESSI due to the limited spatial resolution of the instrument. Figure 2 shows the sample coordinates, RHESSI HXR and the 6mHz sunquake egression map, plotted over IRIS SJI MG II data in an effort to demonstrate the spatial alignment between HXR (particle beam), UV ribbons and sunquake impact. Table 1 shows how each sample number relates to a heliocentric position in arcseconds.

Sample Number	Heliocentric Position (x,y)
1	518.219”, 262.000”
2	520.215”, 263.000”
3	522.212”, 262.000”
4	522.212”, 265.000”
5	524.256”, 265.000”
6	526.252”, 263.818”

Table 1: Sample number and the corresponding coordinates in heliocentric units (arcsec).

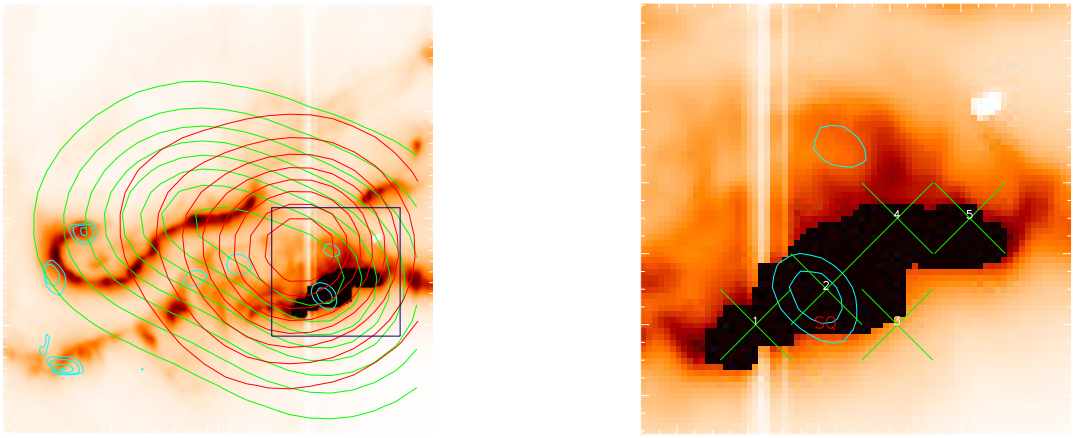

Figure 2: The images show IRIS Mg II slit-jaw data with contours representing HXR emission and 6mHz sunquake power. The black box highlights the area contained in the zoomed plot on the right. The cyan contours show the 6mHz egression power, with the location of the sunquake shown in red on the right. The green and red contours on the left plot show RHESSI HXR data at 25 - 50 and 50 - 100 keV. The green crosses on the right plot show sample positions numbered in accordance with table 1 Each of the IRIS SJ and SDO HMI data sets are sampled at the exact same coordinates in heliocentric units.

1.3 Results and Discussion

1.4 Interpretation and Discussion

1.5 Conclusions and Thesis Plan

References

P. Boerner, C. Edwards, J. Lemen, A. Rausch, C. Schrijver, R. Shine, L. Shing, R. Stern, T. Tarbell, A. Title, C. J. Wolfson, R. Soufli, E. Spiller, E. Gullikson, D. McKenzie, D. Windt, L. Golub, W. Podgorski, P. Testa, and M. Weber. Initial Calibration of the Atmospheric Imaging Assembly (AIA) on the Solar Dynamics Observatory (SDO). Sol. Phys., 275:41–66, January 2012. doi: 10.1007/s11207-011-9804-8.

J. C. Brown. The Deduction of Energy Spectra of Non-Thermal Electrons in Flares from the Observed Dynamic Spectra of Hard X-Ray Bursts. Sol. Phys., 18:489–502, July 1971. doi: 10.1007/BF00149070.

S. Couvidat, J. Schou, R. A. Shine, R. I. Bush, J. W. Miles, P. H. Scherrer, and R. L. Rairden. Wavelength Dependence of the Helioseismic and Magnetic Imager (HMI) Instrument onboard the Solar Dynamics Observatory (SDO). Sol. Phys., 275:285–325, January 2012. doi: 10.1007/s11207-011-9723-8.

B. De Pontieu, A. M. Title, J. R. Lemen, G. D. Kushner, D. J. Akin, B. Allard, T. Berger, P. Boerner, M. Cheung, C. Chou, J. F. Drake, D. W. Duncan, S. Freeland, G. F. Heyman, C. Hoffman, N. E. Hurlburt, R. W. Lindgren, D. Mathur, R. Rehse, D. Sabolish, R. Seguin, C. J. Schrijver, T. D. Tarbell, J.-P. Wülser, C. J. Wolfson, C. Yanari, J. Mudge, N. Nguyen-Phuc, R. Timmons, R. van Bezooijen, I. Weingrod, R. Brookner, G. Butcher, B. Dougherty, J. Eder, V. Knagenhjelm, S. Larsen, D. Mansir, L. Phan, P. Boyle, P. N. Cheimets, E. E. DeLuca, L. Golub, R. Gates, E. Hertz, S. McKillop, S. Park, T. Perry, W. A. Podgorski, K. Reeves, S. Saar, P. Testa, H. Tian, M. Weber, C. Dunn, S. Eccles, S. A. Jaeggli, C. C. Kankelborg, K. Mashburn, N. Pust, L. Springer, R. Carvalho, L. Kleint, J. Marmie, E. Mazmanian, T. M. D. Pereira, S. Sawyer, J. Strong, S. P. Worden, M. Carlsson, V. H. Hansteen, J. Leenaarts, M. Wiesmann, J. Aloise, K.-C. Chu, R. I. Bush, P. H. Scherrer, P. Brekke, J. Martinez-Sykora, B. W. Lites, S. W. McIntosh, H. Uitenbroek, T. J. Okamoto, M. A. Gummin, G. Auker, P. Jerram, P. Pool, and N. Waltham. The Interface Region Imaging Spectrograph (IRIS). Sol. Phys., 289:2733–2779, July 2014. doi: 10.1007/s11207-014-0485-y.

G. S. Kerr and L. Fletcher. Physical Properties of White-light Sources in the 2011 February 15 Solar Flare. ApJ, 783:98, March 2014. doi: 10.1088/0004-637X/783/2/98.